International Journal of Earth Sciences
https://doi.org/10.1007/s00531-022-02164-7

ORIGINAL PAPER

Maturation of East Junggar oceanic arc related to supracrustal recycling driven by arc–arc collision: perspectives from zircon Hf–O isotopes

Yunying Zhang[1,2,3] · Min Sun[3] · Jiyuan Yin[4] · Chao Yuan[5] · Zhen Sun[1,2] · Xiaoping Xia[5]

Received: 29 June 2021 / Accepted: 19 January 2022

Abstract

Oceanic arcs are crucial sites for producing new continental crust. However, how the continental crust has acquired its bulk "andesitic to dacitic" compositions is not well-understood. To address this issue, we carry out an integrated study for granitoids from the East Junggar oceanic arc, Central Asian Orogenic Belt. All the granitoid samples with ages of 332–280 Ma have high SiO_2 but low MgO contents, indicating a dominant crustal source. Based on zircon O isotopes, these granitoids can be divided into three groups: Group I (5.0 ± 0.46‰, 2SD), Group II (8.6 ± 0.47–9.4 ± 0.52‰, 2SD) and Group III (6.8 ± 0.36–7.4 ± 0.48‰, 2SD) with mantle-like, elevated and intermediate zircon $\delta^{18}O$ ratios, respectively. The formation of Group I granitoids can be ascribed to partial melting of juvenile mafic crust, while Group II and III granitoids were likely derived from a mixed source of juvenile mafic crust and supracrustal rocks in variable proportions. Combined with their depleted mantle-like zircon εHf(t) values (+ 11.6 to + 13.5), it is inferred that these supracrustal rocks were mainly isotopically unevolved, immature volcanogenic sediments. The zircon Hf–O isotope array is compatible with mixing between juvenile mafic crust and supracrustal volcanics (40–70% for Group II and 20–40% for Group III) in their magma sources. The incorporation of supracrustal rocks into such high-$\delta^{18}O$ granitoids was likely associated with fore-/intra-arc basin closure triggered by arc–arc collision. Our results thus highlight the role of supracrustal recycling induced by collisional events in driving the compositional differentiation of oceanic arc crust from basaltic to felsic.

Keywords Oceanic arc maturation · Supracrustal recycling · Arc–arc collision · Zircon Hf–O isotopes · East Junggar oceanic arc

Introduction

The "chemically evolved" continental crust is the Earth's unique feature in comparison with other known terrestrial planets (Rudnick 1995). Given the similarity of trace element patterns between continental crust and arc magmas and the depleted mantle-like radiogenic isotopes of oceanic arc lavas, it is accepted that oceanic arcs are critical sites for production of modern continental crust (Stern 2002; Dhuime et al. 2011; Jagoutz and Kelemen 2015). However, primitive arc lavas in oceanic arcs are mainly basaltic, which contrasts with the bulk "andesitic to dacitic" compositions of the continental crust (e.g., Rudnick and Gao 2003). To fill up this compositional gap, an additional process responsible for the compositional differentiation of oceanic arc crust from basaltic to felsic is required. Most of the proposed models commonly involve a two-step process, namely the extraction of mafic magmas by mantle melting and intracrustal

✉ Jiyuan Yin
yinjiyuan1983@163.com

1 Key Laboratory of Ocean and Marginal Sea Geology, South China Sea Institute of Oceanology, Innovation Academy of South China Sea Ecology and Environmental Engineering, Chinese Academy of Sciences, Guangzhou 510301, China

2 Southern Marine Science and Engineering Guangdong Laboratory, Guangzhou 511458, China

3 Department of Earth Sciences, The University of Hong Kong, Pokfulam Road, Pok Fu Lam, Hong Kong, China

4 Key Laboratory of Deep-Earth Dynamics of Ministry of Natural Resources, Institute of Geology, Chinese Academy of Geological Sciences, Beijing 100037, China

5 State Key Laboratory of Isotope Geochemistry, Guangzhou Institute of Geochemistry, Chinese Academy of Sciences, Guangzhou 510640, China

Published online: 05 February 2022

differentiation by remelting and/or fractional crystallization of those mafic rocks (Hawkesworth and Kemp 2006; Lee and Bachmann 2014). Nevertheless, the role of recycling of supracrustal rocks is largely uncertain (Roberts et al. 2013). As the major constituent of the continental crust, granitoids dominate the chemical compositions of the upper continental crust and thus those formed in intra-oceanic arcs bear the critical information about whether supracrustal rocks play a role in the differentiation of oceanic arc crust.

Zircon is a common accessory mineral in granitic rocks and contains a wealth of isotopic (e.g., Lu–Hf and O) information, thus being an ideal recorder of isotopic compositions of the magma sources (Valley et al. 2005). While Lu–Hf is a radiogenic isotope system and can discern recycled crustal components if they are old enough to have measurable ingrowth of radiogenic daughter isotopes (Griffin et al. 2002), it cannot discriminate between supracrustal and intracrustal components in the granitic sources in the intra-oceanic arc setting, because both two components are juvenile and have similar Lu–Hf isotopes inherited from the pristine mantle source (e.g., Jeon et al. 2014). In contrast, zircon O isotopes have the potential to identify the contributions of supracrustal rocks, as O isotopes are fractionated and $\delta^{18}O$ values are elevated during low-temperature surficial processes (Peck et al. 2000; Spencer et al. 2014). Generally, zircons in equilibrium with magmas from the pristine mantle or juvenile mafic crust have mantle-like $\delta^{18}O$ values ($5.3 \pm 0.6‰$, 2SD; Valley et al. 1998; Page et al. 2007), whereas incorporation of supracrustal components in the granitic sources will make zircon $\delta^{18}O$ values deviate from the mantle range (Kemp et al. 2007). Therefore, the combination of Hf with O isotopic studies on zircons could discern the contributions of supracrustal components to the magma sources and provide information about the recycled supracrustal components.

The Central Asian Orogenic Belt (CAOB), situated between the Siberian Craton to the north and the North China–Tarim cartons to the south (Fig. 1a), is one of the largest accretionary orogenic belts on the Earth (Sengör et al. 1993; Windley et al. 2007). It was formed through

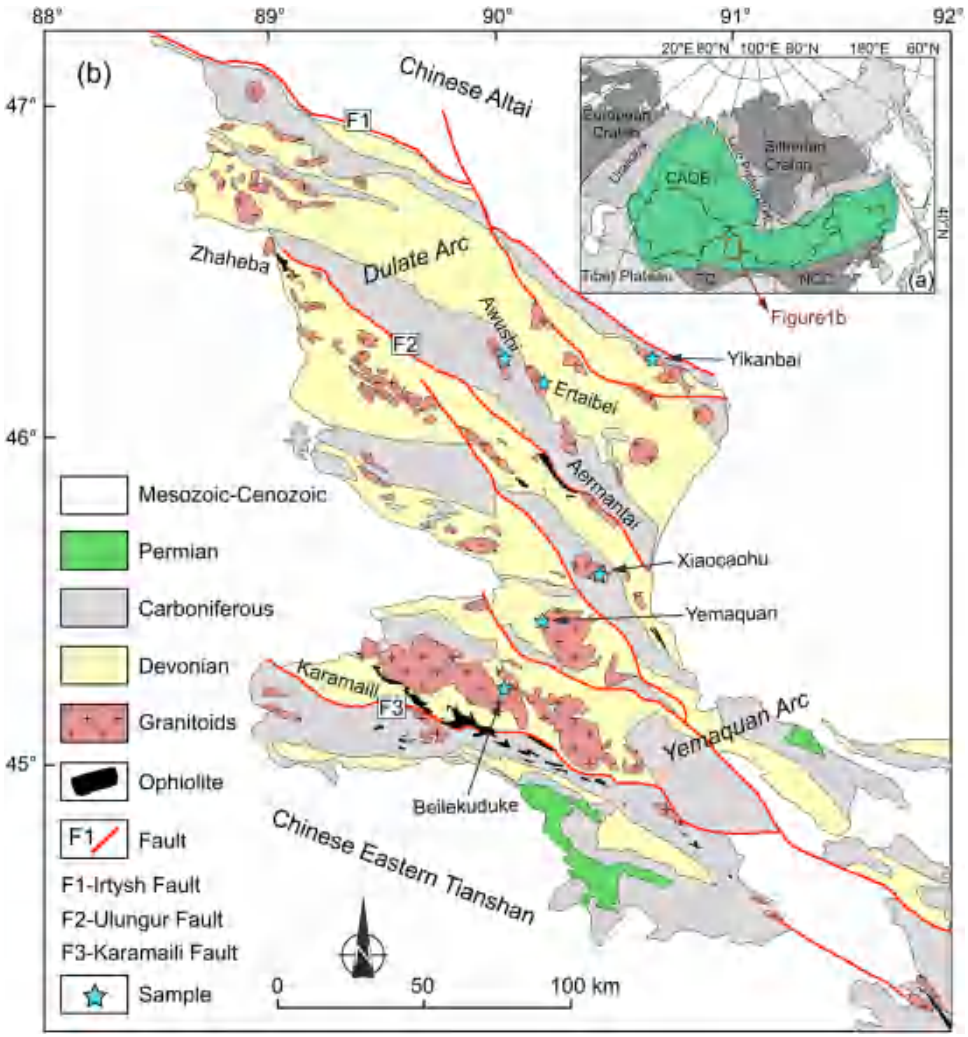

Fig. 1 **a** Simplified tectonic map of the CAOB (modified after Jahn et al. 2000) and **b** geological map of the east Junggar (modified after Liu et al. 2013) showing sample locations. *TC* Tarim Craton, *NCC* North China Craton

multiple subduction-accretion processes as a result of successive closure of the Paleo-Asian Ocean and is composed of massive juvenile terranes including island arc-back arc systems, accretionary wedges and ophiolitic mélanges (Wilhem et al. 2012; Zhang et al. 2018). The East Junggar occupies the southern part of the CAOB (Fig. 1), represents a typical intra-oceanic arc and is featured by voluminous volcanogenic sediments and granitoid rocks (Han et al. 1997; Xiao et al. 2004; Tang et al. 2017). Ascertaining the petrogenesis of these granitoids holds the key to understanding the differentiation process of oceanic arc crust. This study presents high-precision zircon U–Pb–Hf–O isotopic and bulk-rock geochemical data for the late Paleozoic granitoids from the East Junggar, and these results allow us to determine their petrogenesis and source components, and to further constrain the differentiation process of oceanic arc crust.

Regional geological background

The East Junggar, separated from the Chinese Altai to the north by the Irtysh Fault and from the Chinese Eastern Tianshan to the south by the Karamaili ophiolitic belt (Fig. 1b), represents a Paleozoic intra-oceanic island arc system in the CAOB (Xiao et al. 2004; An et al. 2021). This arc system is composed of the Dulate arc and the Yemaquan arc bordered by the Zhaheba–Aermantai ophiolitic mélanges with zircon U–Pb ages of 503–490 Ma (Jian et al. 2003; Xiao et al. 2009; Luo et al. 2017). Studies on the Zhaheba–Aermantai ophiolitic mélanges suggest that these mélanges do not stand the suture between the two arcs but a part of oceanic island arc–ophiolite complex (Luo et al. 2017). With that in mind, the formation of the East Junggar has been thought to be associated with a long-lived (Cambrian to Carboniferous) northward subduction of the Junggar Ocean represented by the Karamaili ophiolitic mélange (Han and Zhao 2018; Zhang et al. 2018). The closure of this oceanic basin probably occurred in the late Carboniferous (ca. 320 Ma) on the basis of the tectono-sedimentary studies across the Karamaili belt (Li et al. 2020). The regional strata mainly includes Devonian to Carboniferous volcanogenic sedimentary rocks (Xiao et al. 2004; Liu et al. 2014; Li et al. 2019). Granitoids with late Devonian to early Permian ages are widespread in the East Junggar and are characterized by high and positive Nd–Hf isotopic values ($\varepsilon Nd(t) = +5$ to $+7$; zircon $\varepsilon Hf(t) = +10$ to $+17$), consistent with an origin in an intra-oceanic arc setting with negligible contribution from old continental crust (Liu et al. 2013; Tang et al. 2017; Aibai et al. 2019; Song et al. 2019).

Sampling and petrology

Six representative granitoid plutons from the East Junggar were sampled for petrological and geochemical investigation and sample locations are shown in Fig. 1b. The Yikanbai pluton is a fine- to medium-grained (0.2–4 mm) granodiorite, which is composed of plagioclase (~45 vol.%), K-feldspar (~25 vol.%), amphibole (~10 vol.%), biotite (~10 vol.%) and quartz (~10 vol.%) with minor apatite and titanite (Fig. 2a, b). Plagioclase grains in this pluton are euhedral, while amphibole and K-feldspar crystals are subhedral. The Ertaibei pluton is a fine- to medium-grained (0.2–5 mm) granodiorite, made up of plagioclase (~45 vol.%), K-feldspar (~25 vol.%), amphibole (~10 vol.%), biotite (~5 vol.%) and quartz (10~15 vol.%) with accessory minerals such as apatite, titanite and allanite (Fig. 2c, d). Plagioclase, K-feldspar and biotite crystals show subhedral form. The Awushi pluton is a fine- to medium-grained (0.2–5 mm) K-feldspar granite, comprised of plagioclase (~25 vol.%), K-feldspar (~40 vol.%) and quartz (~30 vol.%) with minor biotite, apatite and allanite (Fig. 2e, f). K-feldspar and plagioclase grains are subhedral in shape, while quartz crystals are anhedral. The Xiaocaohu pluton is a medium-grained (2–5 mm) monzogranite, which is composed mainly of plagioclase (~35 vol.%), K-feldspar (~30 vol.%) and quartz (~30 vol.%) with subordinate amphibole (~3 vol.%) and biotite (~2 vol.%). Accessory minerals are apatite, titanite and allanite (Fig. 2g, h). The Yemaquan pluton is a fine-grained (0.1–2 mm) monzogranite, which consists of plagioclase (~35 vol.%), K-feldspar (~25 vol.%) and quartz (35~40 vol.%) with minor biotite and accessory minerals (e.g., apatite and zircon). Plagioclase grains are subhedral, whereas K-feldspar and quartz crystals are anhedral (Fig. 2i, j). The Beilekuduke pluton is a medium- to coarse-grained (2–7 mm) monzogranite, with mineral assemblage including subhedral plagioclase (30–35 vol.%) and K-feldspar (25–30 vol.%), and anhedral quartz (~35 vol.%) and minor biotite as well as accessory minerals (e.g., apatite and zircon) (Fig. 2k, l).

Analytical methods

Zircon U–Pb–Hf–O isotope analyses

Zircon grains were separated from crushed rocks using the conventional heavy liquid and magnetic techniques, followed by hand-picking under a binocular microscope. Representative zircon crystals were mounted in epoxy resin disks and polished to about half of their thickness. Zircon U−Pb dating for samples EJ1308 and EJ1310 was

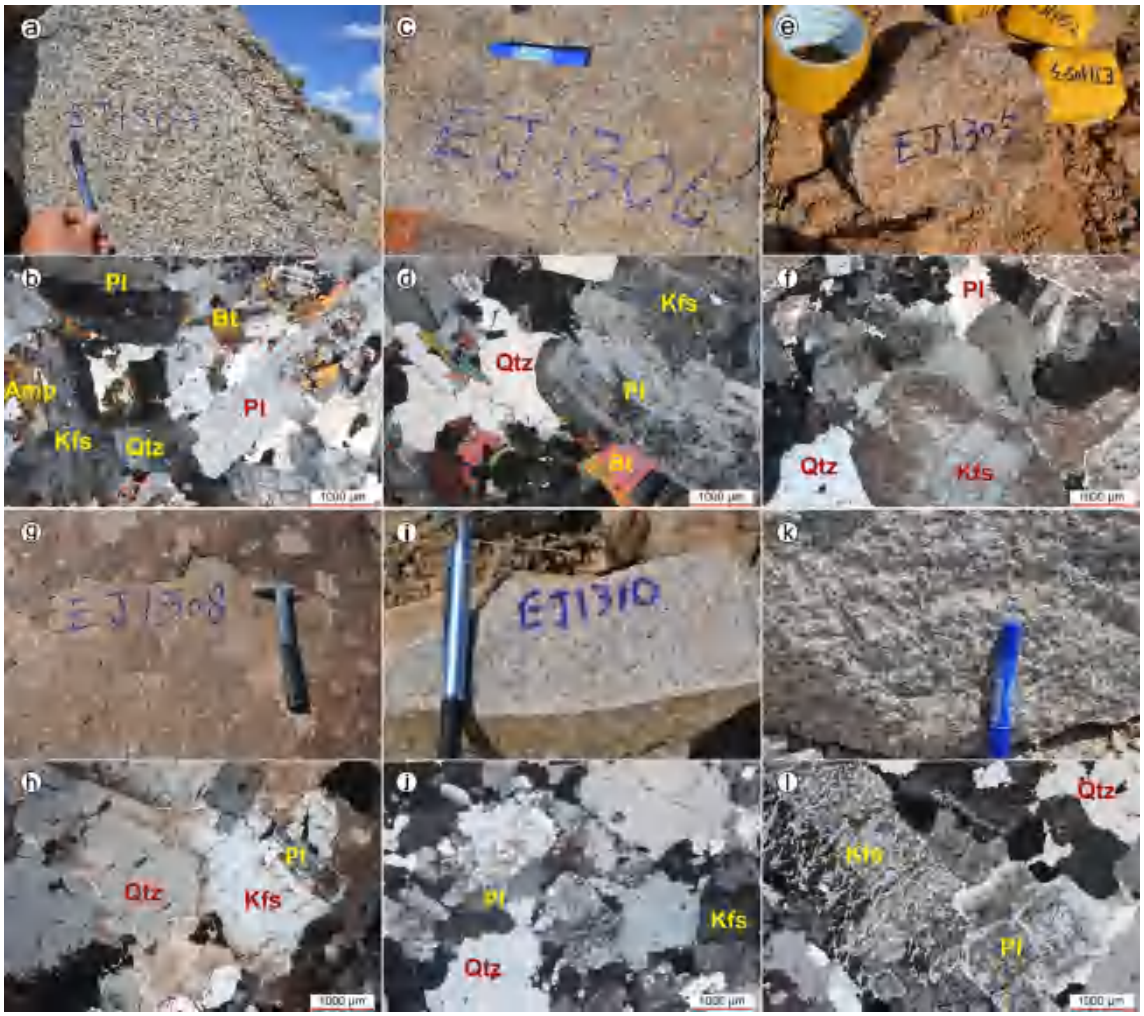

Fig. 2 Photographs of outcrops and photomicrographs showing the geological and mineralogical characteristics of the granitoids from the East Junngar. **a**, **b** Yikanbai granodiorite, **c**, **d** Ertaibei granodiorite, **e**, **f** Awushi K-feldspar granite, **g**, **h** Xiaocaohu monzogranite, **i**, **j** Yemaquan monzogranite and **k**, **l** Beilekuduke monzogranite. *Amp* amphibole, *Pl* plagioclase, *Kfs* K-feldspar, *Bt* biotite, *Qtz* quartz

performed using the MC-ICP-MS (Multi Collector Inductively Coupled Plasma Mass Spectrometry) equipped with a 193 nm excimer ArF Laser Ablation system at the Institute of Geology and Geophysics, Chinese Academy of Sciences (CAS), while that for other samples was conducted by Nu instruments MC-ICP-MS attached to a Resonetics Resolution M-50-HR Excimer Laser Ablation system in the University of Hong Kong. Helium was employed as a carrier gas, and argon was used as the make-up gas and mixed with the carrier gas via a T-connector before entering the ICP. The detailed analytical procedures and instrument parameters for the two techniques were described in Xie et al. (2018) and Xia et al. (2011), respectively. Zircon 91500 was utilized as an external standard to calibrate the U−Th−Pb isotopic ratios and the results yield a weighted mean $^{206}Pb/^{238}U$ age of 1062.4 ± 2.2 Ma ($n = 21$), consistent, within error, with the recommended value of 1062.4 ± 0.8 Ma (Wiedenbeck et al. 1995). In addition, zircon standard GJ-1 was analyzed with our unknown zircons and the results give a weighted mean $^{206}Pb/^{238}U$ age of 607.3 ± 1.0 Ma ($n = 20$) that is identical to the reported result of 610.0 ± 1.7 Ma (Elhlou et al. 2006). Off-line integration of back-ground and analytical signals, and time-drift correction and quantitative calibration were conducted using the ICPMSDataCal 8.0 (Liu et al. 2010). Isoplot 3.0 software was used to process the weighted mean U−Pb ages and concordia diagrams (Ludwig 2003).

In situ zircon Lu−Hf isotopic compositions were measured on the same Nu Plasma MC-ICP-MS in the University of Hong Kong. Analyses were performed with a beam diameter of ca. 55 μm and 6 Hz repetition rate, which gave a signal intensity of 0.04 V at ^{179}Hf for the standard zircon 91500. Data acquisition for each analysis consists of 30 s background collection and 40 s signal collection for

laser ablation. The measured isotopic ratios of $^{176}Hf/^{177}Hf$ were normalized to $^{176}Hf/^{177}Hf = 0.7325$, using an exponential correction for mass bias. Isobaric interference of ^{176}Yb and ^{176}Lu on ^{176}Hf was corrected by monitoring ^{172}Yb and ^{175}Lu, respectively. Ratios used for such corrections were 0.5887 for $^{176}Yb/^{172}Yb$ and 0.02655 for $^{176}Lu/^{175}Lu$ (Vervoort et al. 2004). Standard zircons 91500 and GJ-1 were used as external standards and were analyzed twice before and after every ten analyses. The ^{176}Lu decay constant of 1.867×10^{-11} year^{-1} (Söderlund et al. 2004) was used to calculate initial $^{176}Hf/^{177}Hf$ ratios. The chondritic values of $^{176}Hf/^{177}Hf$ (0.282772) and $^{176}Lu/^{177}Hf$ (0.0332) reported by Blichert-Toft and Albarède (1997) were adopted for the calculation of εHf values. Single-stage Hf model ages (T_{DM1}) were calculated relative to the depleted mantle present-day value of $^{176}Hf/^{177}Hf = 0.283250$ and $^{176}Lu/^{177}Hf = 0.0384$ (Griffin et al. 2000). Two-stage model ages (T_{DM2}) were calculated using the mean $^{176}Lu/^{177}Hf$ ratio of 0.015 for the average continental crust (Griffin et al. 2002).

Zircon oxygen isotope analysis was undertaken by the CAMECA IMS1280-HR SIMS at the Guangzhou Institute of Geochemistry, CAS (GIG, CAS), following the procedures described by Li et al. (2010a). A focused Cs + primary ion beam was accelerated at 10 kV, with an intensity of ~ 2 nA, and the analytical beam diameter is about 10 μm. The measured oxygen isotopic data were corrected for instrumental mass fractionation (IMF) using the Penglai zircon standard ($\delta^{18}O_{VSMOW} = 5.3‰$) (Li et al. 2010b), which was analyzed once every four unknowns. The internal precision of a single analysis was generally better than 0.2‰ (1σ standard error) for the $^{18}O/^{16}O$ ratio. Twenty-eight measurements of Penglai zircon standard during the course of this study yielded a weighted mean of $\delta^{18}O = 5.3 \pm 0.2‰$ (2σ SD), consistent within errors with the reported value of 5.3‰ ± 0.1‰ (2σ SD) (Li et al. 2010b). In addition, eleven measurements of the Qinghu zircon standard in this study gave a weighted mean of $\delta^{18}O = 5.4 \pm 0.3‰$ (2SD), which is in agreement with the reported value of 5.4 ± 0.2‰ (Li et al. 2013).

Bulk-rock major and trace elements

Bulk-rock major and trace element compositions were determined at the GIG, CAS. Major element compositions were measured on fused glass disks using a X-ray fluorescence (XRF) spectrometer (Rigaku 100e) following the analytical procedures described by Li et al. (2006), and the analytical uncertainties for major elements were mostly between 1 and 5%. Trace elements, including rare earth elements (REE), high field strength elements (HFSE) and large ion lithophile elements (LILE), were analyzed by a Perkin-Elmer Sciex ELAN 6000 instrument. Sample powders (~ 40 mg) were dissolved with mixed $HF + HNO_3$ acid in high-pressure Teflon bombs for 48 h in order to ensure complete dissolution of refractory minerals. USGS rock standards W-2, BCR-2, BHVO-2 and AGV-2 and Chinese national rock standards (GSD-9, GSR-1, GSR-2 and GSR-3) were used to calibrate elemental concentrations of the measured samples. The analytical precision was generally better than 5% (Li et al. 2006).

Results

Zircon U–Pb ages

Zircon U–Pb geochronological results are presented in Supplementary Table S1. Five (Yikanbai, Yemaquan, Ertaibei, Awushi and Xiaocaohu) of the six plutons have been processed for zircon U–Pb dating in this study, since the Beilekuduke pluton has been given a highly precise zircon U–Pb age of 302.0 ± 2.0 Ma by Liu et al. (2013). Zircon grains extracted from the five plutons are mostly transparent and subhedral to euhedral with crystal lengths of 50–150 μm and aspect ratios of 1:1–1:3 (Fig. 3). The majority of these zircons show well-developed oscillatory zoning, which, coupled with the high zircon Th/U ratios (0.33–1.05) (Supplementary Table S1), suggest an igneous origin. The analyses of fifteen zircon grains from the Yikanbai pluton give $^{206}Pb/^{238}U$ ages between 329 and 338 Ma, with an early Carboniferous weighted mean age of 332.2 ± 1.4 Ma (Fig. 3a), while eighteen, twenty-two and twenty-three concordant $^{206}Pb/^{238}U$ ages form coherent clusters for the Yemaquan, Ertaibei and Awushi plutons, respectively, yielding late Carboniferous weighted mean ages of 317.2 ± 1.8 Ma, 301.6 ± 1.0 Ma and 302.8 ± 1.1 Ma, respectively (Fig. 3b–d). Twenty-three zircon analyses for the Xiaocaohu pluton yield $^{206}Pb/^{238}U$ ages ranging from 273 to 284 Ma, which form a group and give an early Permian weighted mean age of 280.2 ± 2.0 Ma (Fig. 3e). The weighted mean $^{206}Pb/^{238}U$ age of each pluton is interpreted as its crystallization age.

Zircon Hf–O isotopes

Zircon Hf–O isotopic results are presented in Supplementary Table S2. All of the six plutons have been conducted for zircon Hf–O isotopic analyses. The Yikanbai and Yemaquan plutons possess analogous Hf isotopic compositions, with εHf(t) values from + 9.6 to + 13.9 (average 11.6 ± 2.8, 2SD) and from + 9.8 to + 13.5 (average 11.9 ± 2.4, 2SD), respectively (Fig. 4a). In contrast, the Ertaibei, Awushi, Xiaocaohu and Beilekuduke plutons have relatively higher εHf(t) values, from + 11.5 to + 14.4 (average 12.9 ± 1.7, 2SD), from + 11.3 to + 15.5 (average 13.5 ± 2.4, 2SD), from + 11.6 to + 14.4 (average 13.0 ± 1.9, 2SD) and from + 11.3 to + 15.3 (average 13.1 ± 2.4, 2SD), respectively (Fig. 4a). The Xiaocaohu

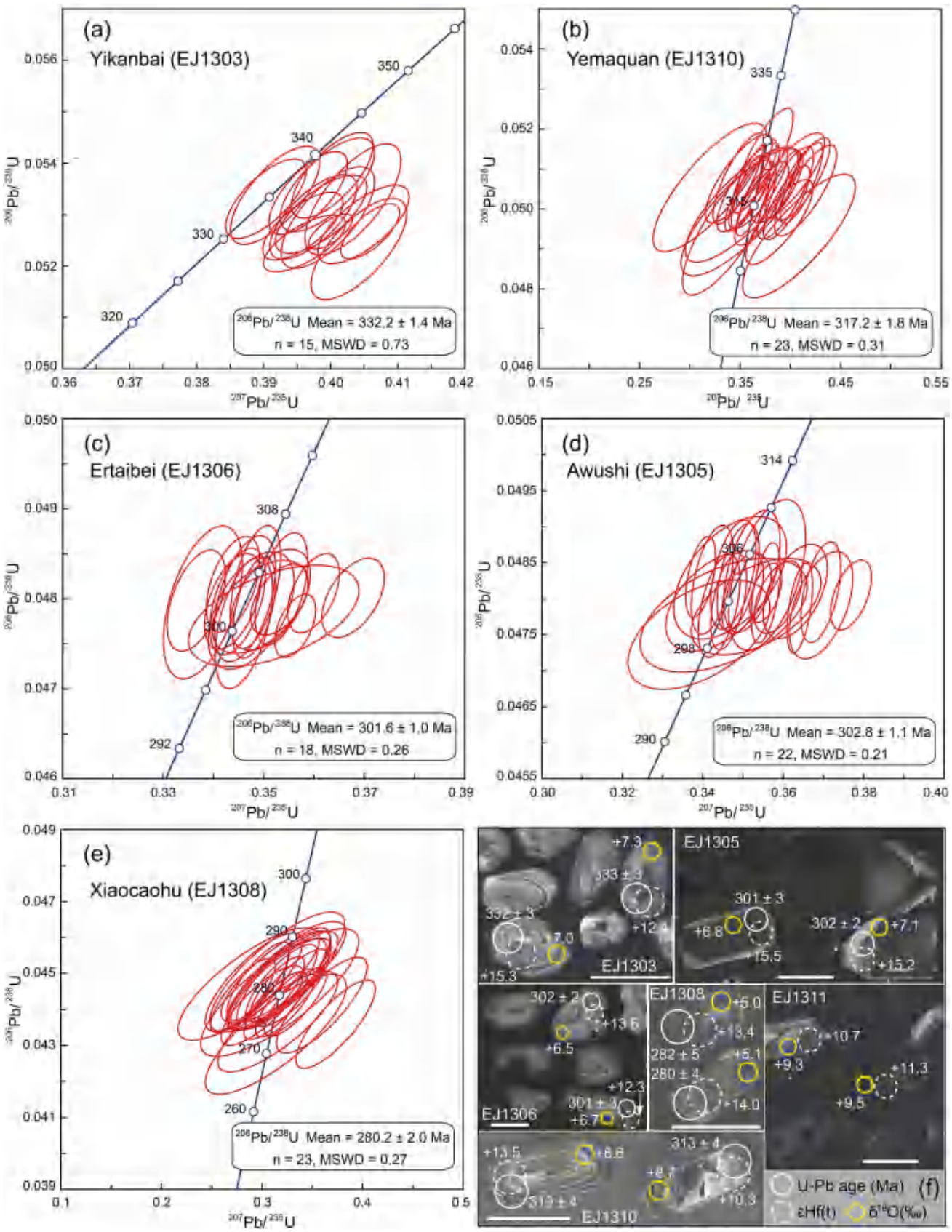
(a)
Yikanbai (EJ1303)
$^{206}Pb/^{238}U$ Mean = 332.2 ± 1.4 Ma
n = 15, MSWD = 0.73
(b)
Yemaquan (EJ1310)
$^{206}Pb/^{238}U$ Mean = 317.2 ± 1.8 Ma
n = 23, MSWD = 0.31
(c)
Ertaibei (EJ1306)
$^{206}Pb/^{238}U$ Mean = 301.6 ± 1.0 Ma
n = 18, MSWD = 0.26
(d)
Awushi (EJ1305)
$^{206}Pb/^{238}U$ Mean = 302.8 ± 1.1 Ma
n = 22, MSWD = 0.21
(e)
Xiaocaohu (EJ1308)
$^{206}Pb/^{238}U$ Mean = 280.2 ± 2.0 Ma
n = 23, MSWD = 0.27
$^{207}Pb/^{235}U$
$^{206}Pb/^{238}U$
EJ1303
EJ1305
EJ1306
EJ1308
EJ1310
EJ1311
U-Pb age (Ma)
εHf(t)
$\delta^{18}O$(‰)
(f)

◂**Fig. 3** **a**–**e** MC-ICP-MS zircon U–Pb concordia plots for the granitoid plutons from the East Junggar. **f** Cathodoluminescence (CL) images of selected zircon crystals showing internal growth zoning and the locations of in-situ isotopic analyses. In (**f**), the scale bars in all CL images are 100 μm in length, the U–Pb ages are presented as $^{206}Pb/^{238}U$ ages, and the errors are quoted at the 2σ level

pluton has zircon $\delta^{18}O$ values of 4.4–5.6‰ with a mean of 5.0 ± 0.46‰ (2SD), resembling those (5.3 ± 0.6‰, 2SD) of igneous zircons in equilibrium with mantle magmas (Valley et al. 1998; Page et al. 2007). Unlike the Xiaocaohu pluton, however, $\delta^{18}O$ values of the Yikanbai [6.9–7.8‰ with a mean of 7.4 ± 0.48‰ (2SD)], Ertaibei [6.4–7.1‰ with a mean of 6.8 ± 0.36‰ (2SD)], Awushi [6.7–7.4‰ with a mean of 7.1 ± 0.42‰ (2SD)], Yemaquan [8.3–9.2‰ with a mean of 8.6 ± 0.47‰ (2SD)] and Beilekuduke [8.0–10.1‰ with a mean of 9.4 ± 0.52‰ (2SD)] plutons are higher than those of mantle-derived zircons (Fig. 4b).

Bulk-rock major and trace elements

Bulk-rock major and trace element compositions are presented in Supplementary Table S3. Samples from the Yikanbai and Ertaibei plutons fall within the granodiorite filed and those from the Awushi, Xiaocaohu, Yemaquan and Beilekuduke plutons can be classified as monzogranite in terms of the Qtz–Or–Pl diagram (Fig. 5a). The Yikanbai and Ertaibei plutons possess intermediate SiO_2 (60.3–60.8 wt.% and 64.6–65.7 wt.%, respectively) and Mg# (43.5–45.0 and 40.1–41.5, respectively) and exhibit metaluminous features with A/CNK [molar $Al_2O_3/(K_2O + Na_2O + CaO)$] values of 0.86–0.89 and 0.87–0.89, respectively, whereas the other four plutons have relatively high SiO_2 (72.8–78.9 wt.%) but low Mg# (2.1–20.5) and show slightly aluminum-rich characteristics (A/CNK = 0.98–1.05) (Fig. 5a, b). All the granitoid plutons are marked by high K_2O (3.96–5.30 wt.%) contents and high K_2O/Na_2O (0.97–1.41) ratios, thus being classified as the high-K calc-alkaline series (Fig. 5c).

The Sr and Ba contents in these plutons are highly variable and show decreasing trends from the Yikanbai and Ertaibei plutons (Sr = 460–712 ppm; Ba = 654–750 ppm) through the Xiaocaohu pluton (Sr = 65.4–76.8 ppm; Ba = 401–438 ppm) to the Awushi, Yemaquan and Beilekuduke plutons (Sr = 4.67–25.2 ppm; Ba = 12.8–116 ppm). Additionally, samples from these plutons display light REE (LREE) enriched patterns (La/Sm = 2.01–7.59) with slightly (δEu of 0.75–0.92 for the Yikaibai and Ertaibei plutons) to strongly (δEu of 0.01–0.33 for the other four plutons) negative Eu anomalies. In the primitive mantle-normalized multi-element diagrams (Fig. 5d), the studied granitoids show negative anomalies of Ba, Nb and Ti and positive anomalies of Rb, Th and U. Distinct from the Sr enrichment in the Yikanbai rocks, rocks from other plutons show Sr depletion (Fig. 5d).

Discussion

Magmatic processes and Source Nature

The evolution of felsic magmas commonly involves fractionation of various minerals such as amphibole, plagioclase, K-feldspar and biotite. Since amphibole preferentially incorporates middle REE (e.g., Dy) over heavy REE (e.g., Yb), its fractionation will introduce a decrease in Dy/Yb ratios (Davidson et al. 2013). Rocks from the Ertaibei and Beilekuduke plutons exhibit decreasing Dy/Yb ratios with declining MgO, implying some fractionation of amphibole (Fig. 6a), while rocks from other plutons do not show evident correlations between Dy/Yb and MgO (Fig. 6a), precluding significant amphibole crystallization. Fractionation of plagioclase and/or K-feldspar will cause characteristic negative Eu anomalies, and discriminating the former from the latter can be made by their tendency to deplete Sr and Sr–Ba, respectively (Hanson 1978). Samples from these plutons display variable negative Eu anomalies (Fig. 6b), which, together with the positive correlation of Ba with Sr for rocks from each individual pluton (Fig. 6c), demonstrate extensive fractionation of K-feldspar. Biotite is another possible crystallization phase, and its fractionation will decrease Rb/Sr and Ba but slightly increase Sr in the residual melts (Rollinson 1993). In log–log diagrams of Ba versus Sr and Rb/Sr versus Sr (Fig. 6c, d), the Sr and Ba contents of these plutons decrease accompanied by increasing Rb/Sr ratios, reflecting negligible fractionation of biotite during the magma evolution.

All of the granitoid plutons in this study have high zircon εHf(t) values (Fig. 4a), comparable to those of new continental crust in modern island arcs (Dhuime et al. 2011), while in terms of zircon O isotopes they can be divided into three groups: Group I (Xiaocaohu pluton), Group II (Beilekuduke and Yemaquan plutons) and Group III (Yikanbai, Ertaibei and Awushi plutons) with low, high and intermediate $\delta^{18}O$ ratios, respectively (Fig. 4a). The Xiaocaohu pluton (Group I) has zircon $\delta^{18}O$ values of 4.4–5.6‰ (average 5.0 ± 0.46‰, 2SD), which are similar to those (5.3 ± 0.6‰, 2SD) of igneous zircons in equilibrium with mantle magmas (Valley et al. 1998; Page et al. 2007). Granitic rocks with zircon $\delta^{18}O$ close to the mantle values can be generated by fractional crystallization of mantle-derived magmas or by melting of intracrustal basaltic rocks (e.g., mafic underplates). The Xiaocaohu pluton has high SiO_2 (72.8–73.5 wt.%), K_2O (5.03–5.17 wt.%) and K_2O/Na_2O (1.21–1.29) but low Mg# (19.8–20.5), thus it was more likely produced by partial melting of intracrustal mafic rocks (e.g., Rapp and Watson

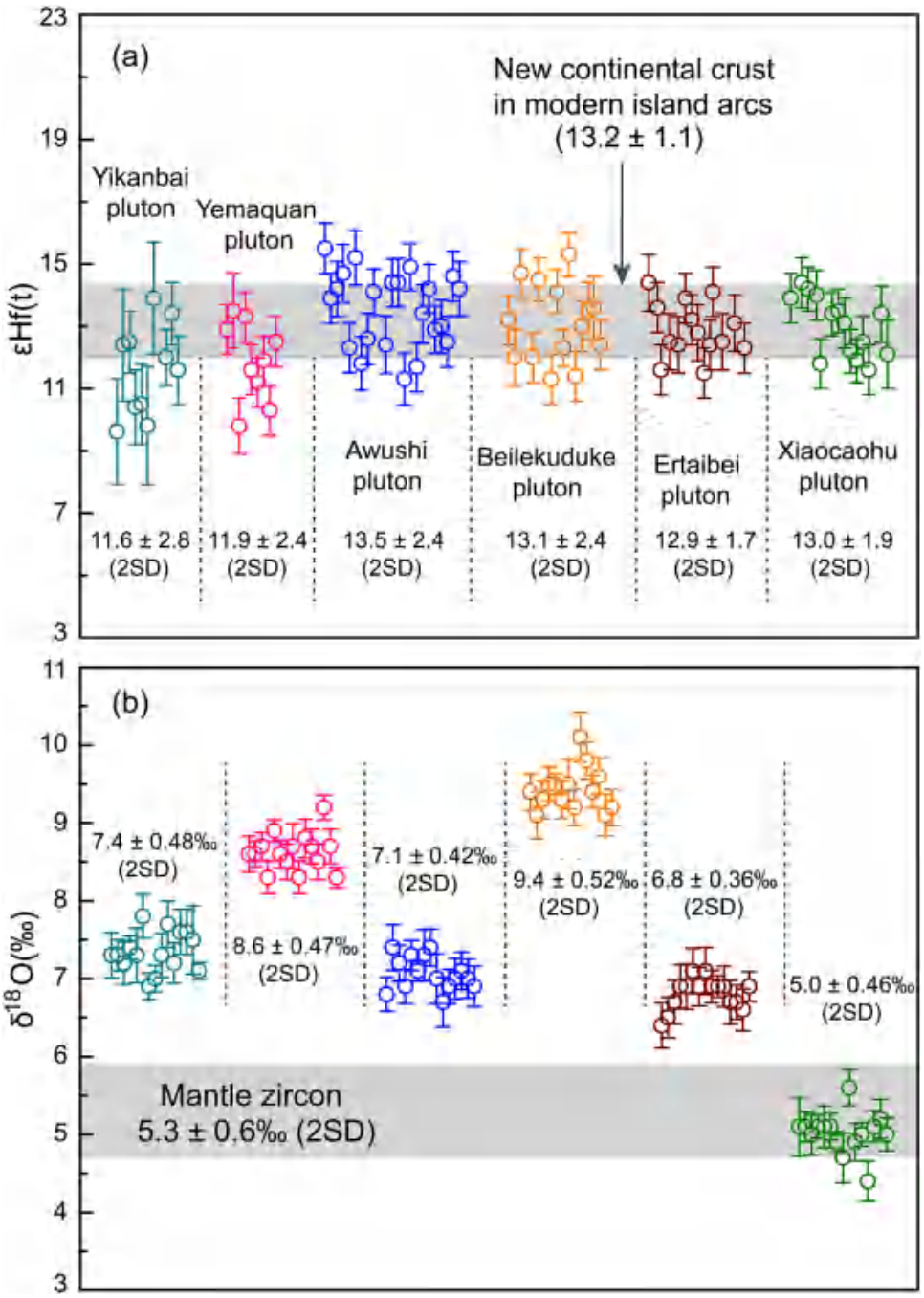

Fig. 4 **a** εHf(t) and **b** $\delta^{18}O$ values of zircons from the studied granitoid plutons in the East Junggar. Error bars represent 2σ of each session. The εHf(t) compositions of new continental crust in modern island arcs are from Dhuime et al. (2011), and the $\delta^{18}O$ range of igneous zircons in equilibrium with mantle magmas is from Valley et al. (1998)

1995). Moreover, its depleted Hf [zircon $\varepsilon Hf(t) = 13.0 \pm 1.9$ (2SD)] isotopic composition suggests a juvenile nature of the source rocks. The reported Carboniferous gabbros in the East Junggar exhibit zircon εHf(t) and $\delta^{18}O$ values analogous to those of the Xiaocaohu pluton (Fig. 7a; Mao et al. 2017; Tang et al. 2020), indicating that they could be the potential counterpart of the source rocks. This inference is further supported by the high K contents for the Xiaocaohu pluton and the medium to high K contents for the Carboniferous gabbros, since it has been experimentally demonstrated that high K granitoids can be generated by melting of medium to high K metabasaltic rocks (Fig. 5c; Sisson et al. 2005).

The zircon $\delta^{18}O$ values of the Yemanquan [$8.6 \pm 0.47‰$ (2SD)] and Beilekuduke [$9.4 \pm 0.52‰$ (2SD)] plutons (Group II) are significantly higher than those of mantle derived rocks but resemble those (8–12‰) of strongly peraluminous leucogranites in the Himalaya that were thought to derive from partial melting of crustal sediments (Hopkinson et al. 2017). Such elevated zircon $\delta^{18}O$ results of the

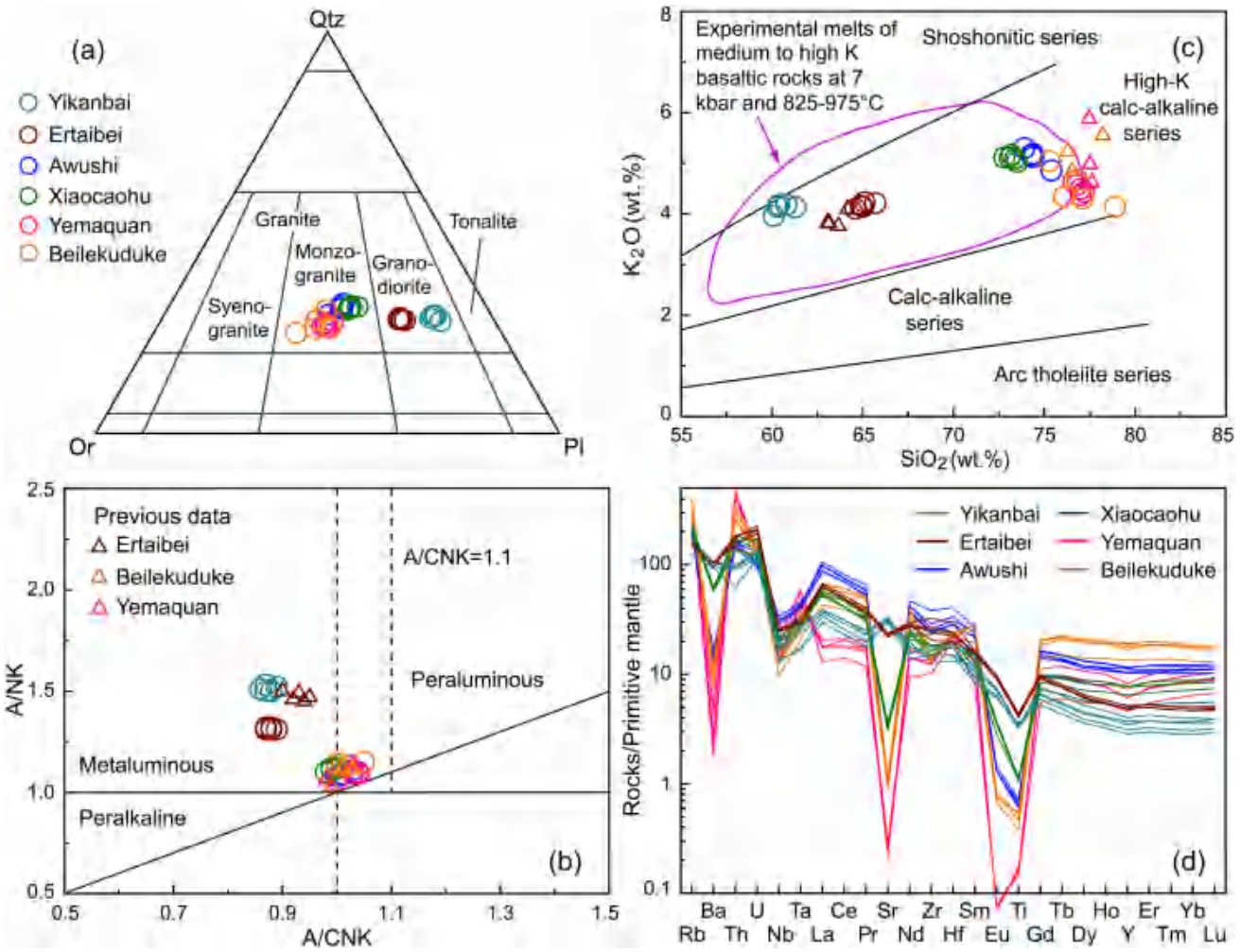

Fig. 5 **a** Classification of the intrusive rocks using CIPW norms (Le Bas and Streckeisen 1991). **b** A/NK–A/CNK diagram (Maniar and Piccoli 1989) and **c** K_2O–SiO_2 (Peccerillo and Taylor 1976) diagrams for the granitoids from the East Junggar. The field for experimental melts of medium to high-K basaltic rocks (7kbar; 825–975 °C) in (**c**) is from Sisson et al. (2005). **d** Primitive mantle-normalized elemental diagrams. The normalizing values are from Sun and McDonough (1989). Previous data for the Ertaibei, Yemaquan and Beilekuduke plutons are from Liu et al. (2013) and Tang et al. (2017)

Group II granitoids thus suggest a dominant supracrustal source, which is consistent with their bulk-rock geochemical compositions such as high SiO_2 (75.3–78.9 wt.%) and Th (22.9–40.4 ppm) contents but low Mg# of 2.1–11.5. On the other hand, their high zircon εHf(t) values (11.9 ± 2.4 to 13.1 ± 2.4) and slightly peraluminous compositions (A/CNK = 1.00–1.05) indicate that the supracrustal source itself was isotopically unevolved and compositionally immature (Kemp et al. 2007; Jeon et al. 2012). Therefore, the young (e.g., Devonian to Carboniferous) basaltic to andesitic volcanogenic sediments of the East Junggar oceanic arc were likely important components in their magma sources, which is in accordance with the widespread development of such rocks in the East Junggar (Zhang et al. 2009; Li et al. 2016). Also, this interpretation is supported by the similar Sr–Nd isotopic compositions between the Yemanquan and Beilekuduke plutons and the Devonian to Carboniferous volcanic rocks (Fig. 7b).

Granitoid plutons of Group III have zircon $\delta^{18}O$ values from 6.8 ± 0.36 to 7.4 ± 0.48‰ (2SD), falling between those of Group I and Group II granitoids (Figs. 4b and 7a). Igneous rocks formed by differentiation of mantle magmas or by melting of juvenile mafic crust tend to crystallize zircons with mantle-like $\delta^{18}O$ ratios (Valley et al. 1998), as exemplified by the Group I granitoids. Given this, zircons with $\delta^{18}O > 6.5$‰ in the Group III granitoids suggest that their magma sources must contain ^{18}O-enriched supracrustal materials. The strongly positive zircon εHf(t) values (11.6 ± 2.8 to 13.5 ± 2.4) and metaluminous to weakly peraluminous compositions (A/CNK = 0.86–1.03) manifest that the involved supracrustal components were probably young, immature volcanogenic sediments. Compared to

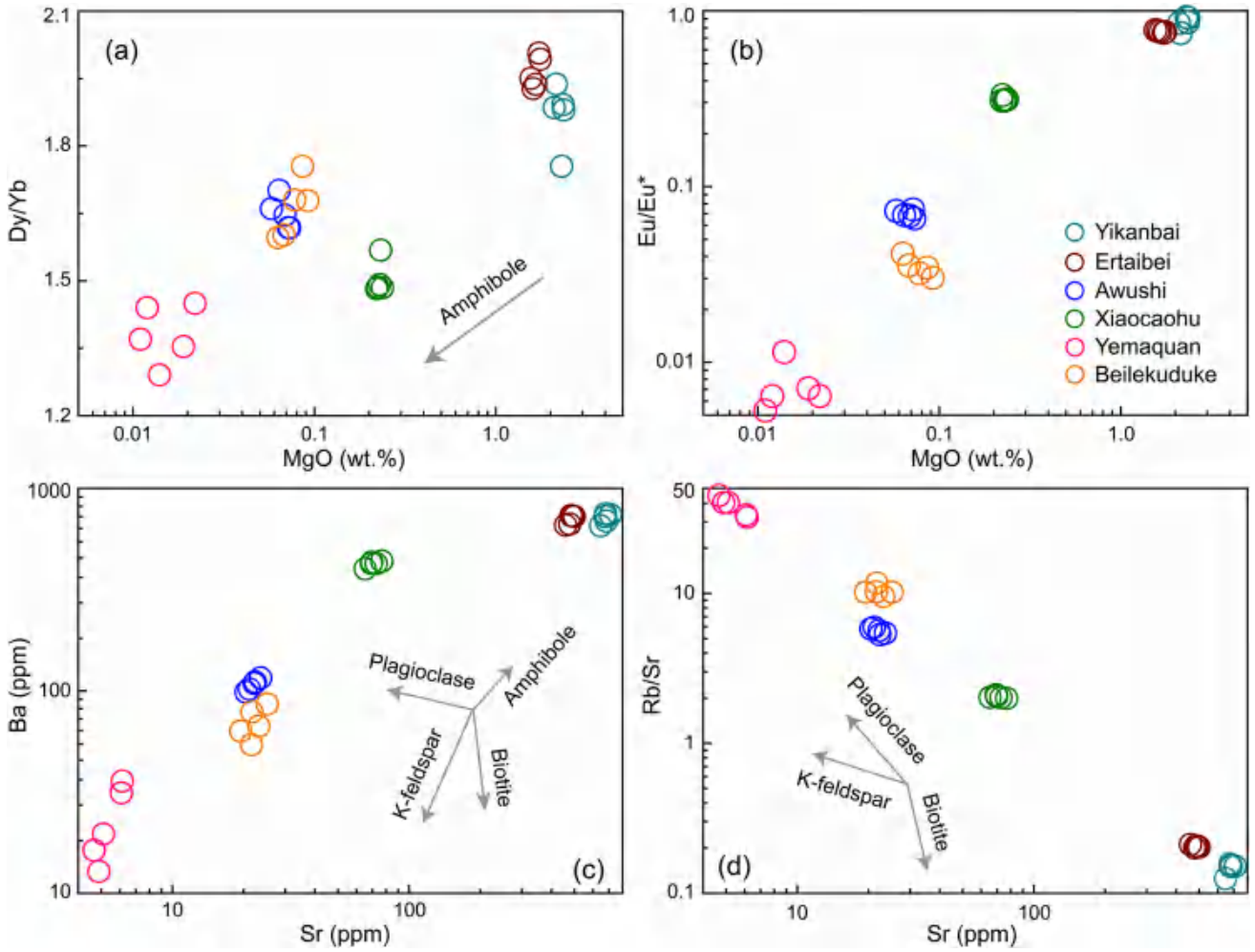

Fig. 6 **a** Dy/Yb–MgO, **b** Eu/Eu*–MgO, **c** Ba–Sr and **d** Rb/Sr–Sr diagrams for the studied granitoids from the East Junggar

pure sediment-derived granitoids (Hopkinson et al. 2017) and Group II granitoids of this study, however, Group III granitoids exhibit relatively lower $\delta^{18}O$ values, pointing to that a relatively low-$\delta^{18}O$ component (mantle-derived magmas or juvenile mafic crust) existed in their magma sources. The low to medium Mg# (6.5–8.3, 40.1–41.5 and 43.5–45.0 for the Awushi, Ertaibei and Yikanbai plutons, respectively) of Group III granitoids are generally consistent with those (Mg# < 41) of experimental products of metabasalts (Rapp and Watson 1995; Sisson et al. 2005), thus indicating that the low-$\delta^{18}O$ end-member was mainly related to melting of juvenile mafic crust despite the possible incorporation of minor mantle magmas into the Yikanbai pluton. This interpretation is compatible with the absence of a pristine mantle signature in the zircon $\delta^{18}O$ data for the Group III granitoids (Appleby et al. 2008). Collectively, Group III granitoids were most likely derived from a mixed source composed mainly of supracrustal materials and juvenile mafic crust.

A binary mixing calculation using zircon Hf–O isotopic data shows that partial melting of a mixed source including young supracrustal volcanogenic sediments and juvenile rocks could reproduce the observed geochemical variations of the granitoids of this study (Fig. 7a). The result suggests a contribution of 40–70% and 20–40% from the supracrustal volcanogenic sediments in the sources of Group II granitoids and Group III granitoids, respectively.

Supracrustal recycling

The incorporation of supracrustal volcanogenic sediments into magmas can be achieved via upper-crustal contamination or deeper-crustal mixing (Peck et al. 2000; Appleby et al. 2008; Jones et al. 2015). However, the lack of xenocrystic zircons and xenoliths of sedimentary origin together with relatively homogeneous zircon $\delta^{18}O$ values within individual pluton does not support the upper-crustal contamination. Actually, magmas ascending to the upper-crustal levels are

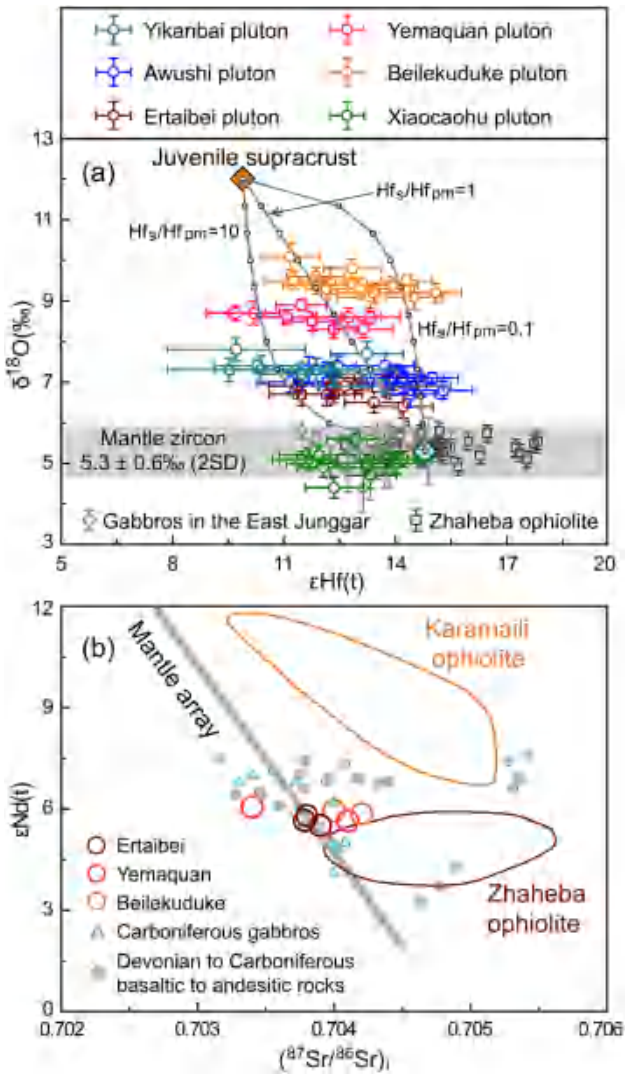

Fig. 7 **a** Zircon $\delta^{18}O$ versus εHf(t) diagram for the studied granitoids in the East Junggar. The curves denote the two component mixing trends between the mantle (or juvenile mafic crust) and juvenile supracrust. Mantle 2013 source has εHf(t) = 15.0 and $\delta^{18}O = 5.3$, and juvenile supracrust has εHf(t) = 10.0 and $\delta^{18}O = 11.0$. Hf_s/Hf_{pm} is the ratio of Hf concentration in the supracurstal (s) melt over parental mantle magma (pm), and the small circles on the curves represent 10% mixing increments. The fields of mantle-derived zircons (Valley et al. 1998) and the Zhaheba ophiolites in the East Junggar (Ye et al. 2017) are shown for comparison. Data for Carboniferous gabbros are from Mao et al. (2017) and Tang et al. (2020) and data for granitoids of previsous studies are from Liu et al. (2016), Aibai et al. (2019), Liu et al. (2019) and Tang et al. (2019, 2020). **b** $_{Nd}(t)$ versus $(^{87}Sr/^{86}Sr)_i$ plot for the igneous rocks from the East Junngar. The data for the Ertaibei, Yemaquan and Beilekuduke plutons are from Liu et al. (2013) and Tang et al. (2017). Data for Carboniferous gabbros are from Tang et al. (2017, 2020) and data for Devonian to Carboniferous basaltic to andesitic rocks are from Zhang et al. (2009), Li et al. (2014) and Liu and Liu (2014). The Karamaili and Zhaheba opiolitic data are from Liu et al. (2017) and Ye et al. (2017)

energetically insufficient to assimilate such high (> 20%) proportions of supracrustal components. Instead, the transport of ^{18}O-enriched supracrustal materials into deeper-crustal zones is feasible. Also, a deeper-crustal melting-mixing process has the potential to dissolve zircons from the supracrustal components within the melts (Roberts et al. 2013). The input of supracrustal rocks into deeper-crust may have occurred via underthrusting during preceding subduction (Lackey et al. 2005, 2008) or tectonic burial by closure of back-arc basins (Kemp et al. 2007, 2009) or by arc–arc collision (Saito et al. 2012). The first process has been invoked to interpret the high-$\delta^{18}O$ Sierra Nevada batholith in the North America arc, where supracrustal rocks were subducted and/or underthrust beneath the arc sometime in the Paleozoic to Jurassic; the second and third processes have been applied to the high-$\delta^{18}O$ granitoids in the Lachlan Fold Belt in SE Australia and the Izu Zone in central Japan, respectively, where supracrustal components were buried during the closure of back-arc basins and arc–arc collision, respectively. Given the intrusion of high-$\delta^{18}O$ granitoids into the potential volcanogenic sedimentary sources (Fig. 1b), the mechanism of tectonic burial may have played a dominant role in transporting the supracrustal rocks into the deep crust in the East Junggar (Tang et al. 2019; Li et al. 2020). Detrital zircon populations of Silurian to Carboniferous sediments from the East Junggar show fore-arc or intra-arc depositional environments on a cumulative probability plot (Fig. 8a), indicating that the potential supracrustal source components were likely deposited in fore-arc or intra-arc basins. Considering that the tectonic transition from subduction to post-collision in the East Junggar occurred in the middle Carboniferous (330–320 Ma; Li et al. 2020) and high-$\delta^{18}O$ granitoids formed mainly after ca. 320 Ma (Fig. 8b), it is reasonable to speculate that the burial and subsequent melting of volcanogenic sediments was associated with the closure of fore/intra-arc basins induced by the collisional events. As a result, melting of such supracrustal materials contributed to the high-$\delta^{18}O$ granitoids in the East Junggar. This scenario is supported by the fact that zircon $\delta^{18}O$ values of granitoids in the East Junggar culminate at ~ 300 Ma (Fig. 8b), consistent with the accumulated burial by collision (e.g., Tang et al. 2019).

Implications for crustal growth and maturation

The CAOB is widely known for its production of voluminous juvenile crust in the Phanerozoic (e.g., Sengör et al. 1993; Jahn et al. 2000). Granitoids with strongly depleted Sr–Nd–Hf isotopic compositions have been served as powerful evidence for crustal growth (i.e., new crust is formed from depleted mantle sources), because such characteristic granitoids could be derived directly from a mantle source or formed by prompt remelting of juvenile mafic crust (e.g., Han et al. 1997). However, zircons from Group II granitoids

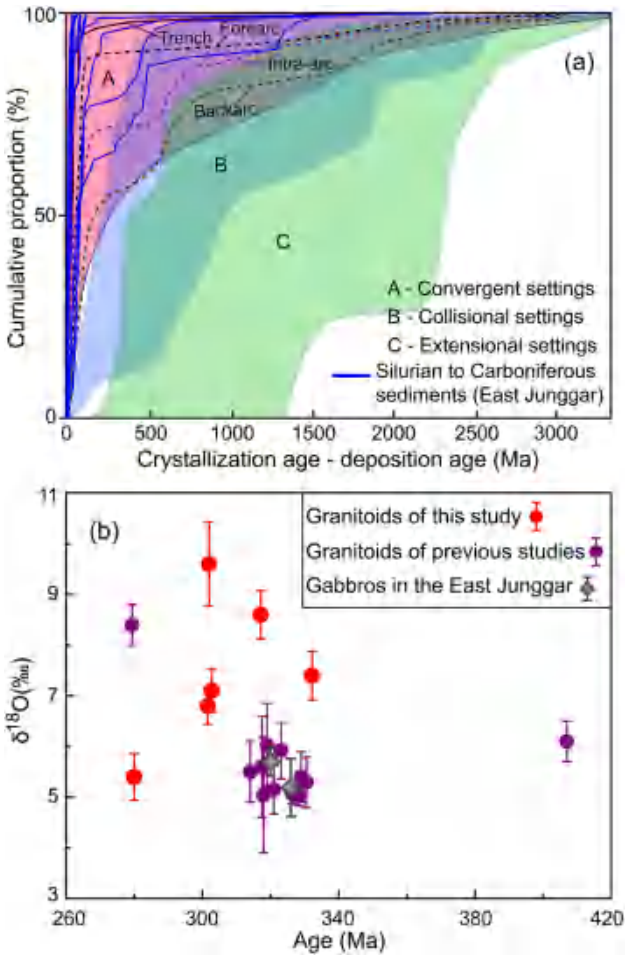

Fig. 8 **a** Cumulative proportion curves of zircon ages for Silurian to Carboniferous sediments from the East Junggar, shown relative to the differences between crystallization ages and deposition ages. Fields and curves for various tectonic settings are after Cawood et al. (2012). Data for Silurian to Carboniferous sediments from the East Junggar are from Li et al. (2019) and references therein. **b** $\delta^{18}O$–Age plot for the igneous rocks from the East Junngar. Data for Carboniferous gabbros are from Mao et al. (2017) and Tang et al. (2020) and data for granitoids of previsous studies are from Liu et al. (2016), Aibai et al. (2019), Liu et al. (2019) and Tang et al. (2019, 2020)

of this study exhibit $\delta^{18}O$ values comparable to those of Himalayan leucogranites (Hopkinson et al. 2017) and possess depleted mantle-like εHf(t) values, implying a significant (40–70%) contribution from recycled, juvenile supracrustal components in their sources. Compared to Group II granitoids, Group III ones have zircon $\delta^{18}O$ values much closer to the range of mantle magmas or juvenile mafic crust, indicating a less proportion (20–40%) of supracrustal rocks in their sources. The zircon $\delta^{18}O$ results of this study thus demonstrate that these granitoids were mainly originated from juvenile crustal sources that contain abundantly supracrustal arc-derived volcanogenic sediments, reflecting that their source rocks were generated during previously accretionary events (e.g., magma underplating during early subduction) and had experienced recycling processes rather than directly from a mantle source. In terms of the scale of orogenic belt evolution, the combination of the studied granitoids with their source rocks points to significant production of new continental crust and thus substantial crustal growth for the CAOB. However, from the perspective of magmatic events, the studied granitoids might predominantly reflect intra-crustal differentiation and thus limited contribution of crustal growth to the CAOB during the periods of granite formation.

Intermediate-acidic rocks make up a major constituent of the upper continental crust (Rudnick and Gao 2003), thus the dioritic to granitoid rocks in the East Junggar of this study record the production of continental crust in an oceanic arc setting. The proposed mechanisms for producing granitoid magmas in oceanic arcs include (1) partial melting of subducting oceanic crust with subsequent interaction with mantle wedge (Kelemen 1995; Rudnick 1995) and (2) fractional crystallization of basaltic melts or partial melting of juvenile mafic crust (Hawkesworth and Kemp 2006; Lee and Bachmann 2014). These mechanisms may all have operated to some extent over the Earth's history. The first mechanism may be more common in the Archean due to the high geothermal gradient (Martin 1999). Partial melting of juvenile mafic crust has contributed to the maturation of East Junggar oceanic arc crust, as evidenced by the formation of Group I granitoids. Distinct from Group I granitoids, the magma sources of the volumetrically abundant Group II and III granitoids involved massive supracrustal rocks, reflecting substantial supracrustal recycling. As discussed above, supracrustal recycling in the East Junggar has occurred via the burial and subsequent melting of volcanogenic sediments, as a response to collision-induced fore/intra-arc basin closure (Fig. 9), highlighting its role in producing high-$\delta^{18}O$ granitoids. The supracrustal recycling during the collisional process is similar to the scenario in the Honshu arc, i.e., the collision of the Honshu arc with the Izu-Bonin arc produced granitoids by mixing between melts of metasediments and arc basalts (Saito et al. 2012). Accordingly, our results imply that supracrustal recycling via tectonic burial by fore/intra-arc basin closure associated with arc–arc collision has played a critical role in driving the compositional differentiation of oceanic arc crust from basaltic to felsic.

Conclusions

The studied granitoids in the East Junggar possess high zircon εHf(t) values from 11.6 ± 2.8 (2SD) to 13.5 ± 2.4 (2SD), comparable to those of new continental crust in modern island arcs, suggesting that the source rocks were juvenile. Combined with their mantle-like [5.0 ± 0.46‰ (2SD)]

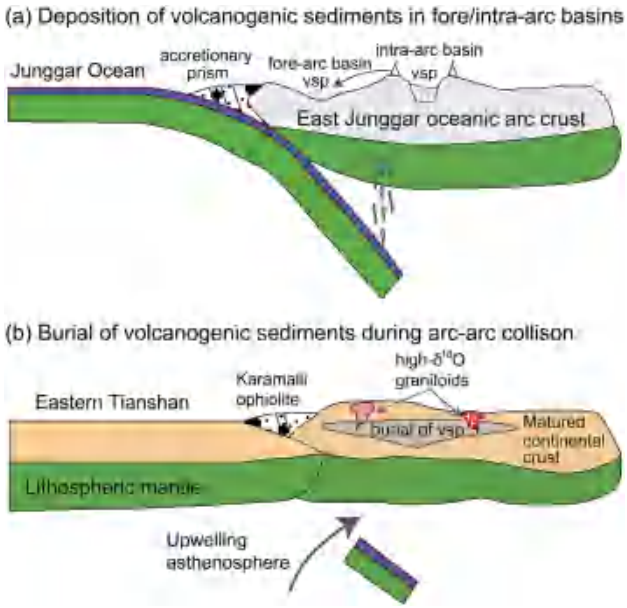

Fig. 9 Schematic cartoons illustrate the burial of volcanogenic sedimentary rocks, subsequent melting of which promote the compositional differentiation of oceanic arc crust from basaltic to felsic. **a** During subduction stage, volcanogenic sedimentary piles (vsp) deposited in the fore/intra-arc basins by weathering of volcanic arc lavas. **b** During collision stage, the vsp were substantially buried, and extensive melting of such vsp gave rise to voluminous high-$\delta^{18}O$ granitoids. The production of high-$\delta^{18}O$ granitoids with incorporation of recycled vsp had driven the differentiation of oceanic arc crust from basaltic to felsic in the East Junggar

to supracrust-like [$9.4 \pm 0.52‰$ (2SD)] $\delta^{18}O$ values, it is implied that most granitoids (i.e., Group II and III granitoids of this study) were generated by anatexis of a mixed source including supracrustal volcanogenic sediments (up to 40–70%) and juvenile mafic crust. These results demonstrate that the recycling and subsequent melting of supracrustal rocks induced by arc–arc collision have played a crucial role in shifting the compositions of oceanic arc crust from basaltic to felsic.

Supplementary Information The online version contains supplementary material available at https://doi.org/10.1007/s00531-022-02164-7.

Acknowledgements We thank Xianglin Tu, Shengling Sun and Jean Wong for their help with the geochemical and geochronological analyses. We appreciate Editor Wolf-Christian Dullo for his kind editorial help and constructive comments. We are grateful to two anonymous reviewers, whose insightful and constructive reviews greatly improve this manuscript. This work is financially supported by the Key scientific issues of transformative technology (2019YFA0708601), the National Key R&D Program of China (2017YFC0601205), the Fund from the Key Laboratory of Deep-Earth Dynamics of Ministry of Natural Resources (J1901-5), the National Science Foundation of China (41873060, 41830216, 41973021), Key Special Project for Introduced Talents Team of Southern Marine Science and Engineering Guangdong Laboratory (Guangzhou) (GML2019ZD0104), Guangdong NSF research team project (No. 2017A030312002), K.C. Wong Education Foundation (GJTD-2018-13), the China Geological Survey (DD20190001, DD20190004) and the Hong Kong RGC research projects (17303415, 17302317). This is a contribution to IGCP 662.

References

Aibai A, Zhang ZC, Cheng ZG, Huang H, Santosh M (2019) Highly differentiated juvenile crust-derived magmas linked with the Xilekuduke porphyry Mo (Cu) deposit in East Junggar. NW China. Ore Geol Rev 115:103103

An R, Zhao GC, Liu Q, Han YG (2021) Early Palaeozoic subduction-accretion in East Junggar (NW China): Insights from age, geochemical, and Sr-Nd-Hf isotopic data of andesitic rocks in the northern Yemaquan Arc. Lithos 380:105892

Appleby SK, Graham CM, Gillespie MR, Hinton RW, Oliver GJH, EIMF (2008) A cryptic record of magma mixing in diorites revealed by high-precision SIMS oxygen isotope analysis of zircons. Earth Planet Sci Lett 269:105–117

Blichert-Toft J, Albarède F (1997) The Lu–Hf isotope geochemistry of chondrites and the evolution of the mantle–crust system. Earth Planet Sci Lett 148:243–258

Cawood PA, Hawkesworth CJ, Dhuime B (2012) Detrital zircon record and tectonic setting. Geology 40:875–878

Davidson J, Turner S, Plank T (2013) Dy/Dy*: variations arising from mantle sources and petrogenetic processes. J Petrol 54:525–537

Dhuime B, Hawkesworth C, Cawood P (2011) When continents formed. Science 331:154–155

Elhlou S, Belousova E, Griffin WL, Pearson NJ, O'Reilly SY (2006) Trace element and isotopic composition of GJ-red zircon standard by laser ablation. Geochim Cosmochim Acta 70:A158

Griffin WL, Pearson NJ, Belousova E, Jackson SE, Achterbergh E, O'Reilly SY, Shee SR (2000) The Hf isotope composition of cratonic mantle: LAM-MC-ICPMS analysis of zircon megacrysts in kimberlites. Geochim Cosmochim Acta 64:133–147

Griffin WL, Wang X, Jackson SE, Pearson NJ, O'Reilly SY, Xu XS, Zhou XM (2002) Zircon chemistry and magma mixing, SE China: in-situ analysis of Hf isotopes, Tonglu and Pingtan igneous complexes. Lithos 61:237–269

Han YG, Zhao GC (2018) Final amalgamation of the Tianshan and Junggar orogenic collage in the southwestern Central Asian Orogenic Belt: constraints on the closure of the Paleo-Asian Ocean. Earth Sci Rev 186:129–152

Han BF, Wang SG, Jahn BM, Hong DW, Kagami H, Sun YL (1997) Depleted-mantle source for the Ulungur River A-type granites from North Xinjiang, China: geochemistry and Nd-Sr isotopic evidence, and implications for Phanerozoic crustal growth. Chem Geol 138:135–159

Hanson GN (1978) The application of trace elements to the petrogenesis of igneous rocks of granitic composition. Earth Planet Sci Lett 38:26–43

Hawkesworth CJ, Kemp AIS (2006) Evolution of the continental crust. Nature 443:811–817

Hopkinson TN, Harris NBW, Warren CJ, Spencer CJ, Roberts NMW, Horstwood MSA, Parrish RR, EIMF (2017) The identification and significance of pure sediment-derived granites. Earth Planet Sci Lett 467:57–63

Jagoutz O, Kelemen PB (2015) Role of arc processes in the formation of continental crust. Annu Rev Earth Planet Sci 43:363–404

Jahn BM, Wu FY, Chen B (2000) Massive granitoid generation in Central Asia: Nd isotope evidence and implication for continental growth in the Phanerozoic. Episodes 23:82–92

Jeon H, Williams IS, Chappell BW (2012) Magma to mud to magma: rapid crustal recycling by Permian granite magmatism

near the eastern Gondwana margin. Earth Planet Sci Lett 319–320:104–117
Jeon H, Williams IS, Bennett VC (2014) Uncoupled O and Hf isotopic systems in zircon from the contrasting granite suites of the New England Orogen, eastern Australia: Implications for studies of Phanerozoic magma genesis. Geochim Cosmochim Acta 146:132–149
Jian P, Liu DY, Zhang Q, Zhang FQ, Shi YR (2003) SHRIMP dating of ophiolite and leucocratic rocks within ophiolite. Earth Sci Front 10:439–456
Jones RE, Kirstein LA, Kasemann SA, Dhuime B, Elliott T, Litvak VD, Alonso R, Hinton R, EIMF (2015) Geodynamic controls on the contamination of Cenozoic arc magmas in the southern Central Andes: insights from the O and Hf isotopic composition of zircon. Geochim Cosmochim Acta 164:386–402
Kelemen PB (1995) Genesis of high Mg# andesites and the continental crust. Contrib Miner Petrol 120:1–19
Kemp AIS, Hawkesworth CJ, Foster GL, Paterson BA, Woodhead JD, Hergt JM, Gray CM, Whitehouse MJ (2007) Magmatic and crustal differentiation history of granitic rocks from Hf–O isotopes in zircon. Science 315:980–983
Kemp AIS, Hawkesworth CJ, Collins WJ, Gray CM, Blevin PL, EIMF (2009) Isotopic evidence for rapid continental growth in an extensional accretionary orogen: the Tasmanides, eastern Australia. Earth Planet Sci Lett 284:455–466
Lackey JS, Valley JW, Saleeby JB (2005) Supracrustal input to magmas in the deep crust of Sierra Nevada batholith: evidence from high-δ^{18}O zircon. Earth Planet Sci Lett 235:315–330
Lackey JS, Valley JW, Chen JH, Stockli DF (2008) Dynamic magma systems, crustal recycling, and alteration in the Central Sierra Nevada Batholith: the oxygen isotope record. J Petrol 49:1397–1426
Le Bas MJ, Streckeisen AL (1991) The IUGS systematics of igneous rocks. J Geol Soc 148:825–833
Lee CT, Bachmann O (2014) How important is the role of crystal fractionation in making intermediate magmas? Insights from Zr and P systematics. Earth Planet Sci Lett 393:266–274
Li XH, Li ZX, Wingate MTD, Chung SL, Liu Y, Lin GC, Li WX (2006) Geochemistry of the 755 Ma Mundine Well dyke swarm, northwestern Australia: part of a Neoproterozoic mantle superplume beneath Rodinia? Precambrian Res 146:1–15
Li XH, Li WX, Li QL, Wang XC, Liu Y, Yang YH (2010a) Petrogenesis and tectonic significance of the 850 Ma Gangbian alkaline complex in South China: evidence from in situ zircon U-Pb dating, Hf-O isotopes and whole-rock geochemistry. Lithos 114:1–15
Li XH, Long WG, Li QL, Liu Y, Zheng YF, Yang YH, Chamberlain KR, Wan DF, Guo CF, Wang XC (2010b) Penglai zircon megacrysts: a potential new working reference material for microbeam determination of Hf–O isotopes and U-Pb age. Geostand Geoanalytical Res 34:117–134
Li XH, Tang GQ, Gong B, Yang YH, Hou KJ, Hu ZC, Li QL, Liu Y, Li WX (2013) Qinghu zircon: a working reference for microbeam analysis of U-Pb age and Hf and O isotopes. Chin Sci Bull 58:4647–4654
Li D, He DF, Santosh M, Tang JY (2014) Petrogenesis of Late Paleozoic volcanics from the Zhaheba depression, East Junggar: insights into collisional event in an accretionary orogen of Central Asia. Lithos 184–187:167–193
Li D, He DF, Tang Y (2016) Reconstructing multiple arc-basin systems in the Altai–Junggar area (NW China): implications for the architecture and evolution of the western Central Asian Orogenic Belt. J Asian Earth Sci 121:84–107
Li PF, Sun M, Shu CT, Yuan C, Jiang YD, Zhang L, Cai KD (2019) Evolution of the Central Asian Orogenic Belt along the Siberian margin from Neoproterozoic-Early Paleozoic accretion to Devonian trench retreat and a comparison with Phanerozoic eastern Australia. Earth Sci Rev 198:102951
Li D, He DF, Sun M, Zhang L (2020) The role of arc-arc collision in accretionary orogenesis: insights from ~320 Ma tectono-sedimentary transition in the Karamaili area, NW China. Tectonics 39:e2019TC005623
Liu XJ, Liu W (2014) Source characteristics and tectonic setting of the Early and Middle Devonian volcanic rocks in the North Junggar, Northwest China: insights from Nd–Sr isotopes and geochemistry. Lithos 184–187:27–41
Liu YS, Hu ZC, Zong KQ, Gao CG, Gao S, Xu J, Chen HH (2010) Reappraisement and refinement of zircon U-Pb isotope and trace element analyses by LA-ICP-MS. Chin Sci Bull 55:1535–1546
Liu W, Liu XJ, Liu LJ (2013) Underplating generated A- and I-type granitoids of the East Junggar from the lower and the upper oceanic crust with mixing of mafic magma: Insights from integrated zircon U-Pb ages, petrography, geochemistry and Nd–Sr–Hf isotopes. Lithos 179:293–319
Liu XJ, Xu JF, Castillo PR, Xiao WJ, Shi Y, Feng ZH, Guo L (2014) The Dupal isotopic anomaly in the southern Paleo-Asian Ocean: Nd–Pb isotope evidence from ophiolites in Northwest China. Lithos 189:185–200
Liu YR, Jian P, Zhang W, Shi YR, Wang YZ, Zhang LQ, Liu DY (2016) Zircon SHRIMP U-Pb dating and O isotope of the Beitashan ophiolitic mélange in the East Junggar, Xinjiang, and its geological significance. Acta Petrol Sin 32:537–554
Liu XJ, Xiao WJ, Xu JF, Castillo PR, Shi Y (2017) Geochemical signature and rock associations of ocean ridge-subduction: evidence from the Karamaili Paleo-Asian ophiolite in east Junggar, NW China. Gondwana Res 48:34–49
Liu XJ, Liu W, Si CQ (2019) Petrogenesis and source rocks of the high-K calc-alkaline and shoshonitic I-type granitoids in the northwestern part of East Junggar, NW China. Lithos 326:298–312
Ludwig KR (2003) User's manual for isoplot 3.00: a geochronological toolkit for microsoft excel, special publication, vol 4. Berkeley Geochronology Center, Berkeley, p 74
Luo J, Xiao WJ, Wakabayashi J, Han CM, Zhang JE, Wan B, Ao SJ, Zhang ZY, Tian ZH, Song DF, Chen YC (2017) The Zhaheba ophiolite complex in Eastern Junggar (NW China): Long lived supra-subduction zone ocean crust formation and its implications for the tectonic evolution in southern Altaids. Gondwana Res 43:17–40
Maniar PD, Piccoli PM (1989) Tectonic discrimination of granitoids. Geol Soc Am Bull 101:635–643
Mao YJ, Tang DM, Qin KZ, Taranovic V (2017) Geochemistry of the ~326 Ma Xinyuan mafic intrusion in the Eastern Junggar Terrane, Northwest China: implications for tectonic setting and magmatic Ni–Cu mineralization potential. Int Geol Rev 59:1276–1291
Martin H (1999) Adakitic magmas: modern analogues of Archaean granitoids. Lithos 46:411–429
Page FZ, Fu B, Kita NT, Fournelle J, Spicuzza MJ, Schulze DJ, Viljoen F, Basei MAS, Valley JW (2007) Zircons from kimberlite: New insights from oxygen isotopes, trace elements, and Ti in zircon thermometry. Geochim Cosmochim Acta 71:3887–3903
Peccerillo A, Taylor SR (1976) Geochemistry of Eocene calc-alkaline volcanic rocks from the Kastamonu area, northern Turkey. Contrib Miner Petrol 58:63–81
Peck WH, King EM, Valley JW (2000) Oxygen isotope perspective on Precambrian crustal growth and maturation. Geology 28:363–366
Rapp RP, Watson EB (1995) Dehydration melting of metabasalt at 8–32 kbar: Implications for continental growth and crust-mantle recycling. J Petrol 36:891–931
Roberts NMW, Slagstad T, Parrish RR, Norry MJ, Marker M, Horstwood MSA (2013) Sedimentary recycling in arc magmas: geochemical and U-Pb–Hf–O constraints on the Mesoproterozoic Suldal Arc, SW Norway. Contrib Miner Petrol 165:507–523

Rollinson HR (1993) Using geochemical data: evaluation, presentation, 922 interpretation. Longman Singapore Publishers (Pte) Ltd., Singapore

Rudnick RL (1995) Making continental crust. Nature 378:573–578

Rudnick RL, Gao S (2003) Composition of the continental crust. In: Rudnick RL (ed) Treatise on geochemistry, 2nd edn. Elsevier, Oxford, pp 1–51

Saito S, Arima M, Nakajima T, Tani K, Miyazaki T, Senda R, Chang Q, Takahashi T, Hirahara Y, Kimura JI (2012) Petrogenesis of the Kaikomagatake granitoids pluton in the Izu Collision Zone, central Japan: implications for transformation of juvenile oceanic arc into mature continental crust. Contrib Miner Petrol 163:611–629

Sengör AMC, Natal'in BA, Burtman VS (1993) Evolution of the Altaid tectonic collage and Palaeozoic crustal growth in Eurasia. Nature 364:299–307

Sisson TW, Ratajeski K, Hankins WB, Glazner AF (2005) Voluminous granitic magmas from common basaltic sources. Contrib Miner Petrol 148:635–661

Söderlund U, Patchett PJ, Vervoort JD, Isachsen CE (2004) The 176Lu decay constant determined by Lu–Hf and U-Pb isotope systematics of Precambrian mafic intrusions. Earth Planet Sci Lett 219:311–324

Song P, Wang T, Tong Y, Zhang JJ, Huang H, Qin Q (2019) Contrasting deep crustal compositions between the Altai and East Junggar orogens, SW Central Asian Orogenic Belt: Evidence from zircon Hf isotopic mapping. Lithos 328:297–311

Spencer CJ, Cawood PA, Hawkesworth CJ, Raub TD, Prave AR, Roberts NM (2014) Proterozoic onset of crustal reworking and collisional tectonics: Reappraisal of the zircon oxygen isotope record. Geology 42:451–454

Stern RJ (2002) Subduction zones. Rev Geophys 40:1012

Sun SS, McDonough WF (1989) Chemical and isotopic systematics of ocean basalt: implications for mantle composition and processes. Geol Soc Lond Spec Publ 42:313–345

Tang GJ, Wang Q, Zhang CF, Wyman DA, Dan W, Xia XP, Chen HY, Zhao ZH (2017) Sr-Nd-Hf-O isotope geochemistry of the Ertaibei pluton, East Junggar, NW China: implications for development of a crustal-scale granitoid pluton and crustal growth. Geochem Geophys Geosyst 18:3340–3358

Tang GJ, Wang Q, Wyman DA, Dan W (2019) Crustal maturation through chemical weathering and crustal recycling revealed by Hf–O–B isotopes. Earth Planet Sci Lett 524:115709

Tang GJ, Wang Q, Wyman DA, Dan W, Ma L, Zhang HX, Zhao ZH (2020) Petrogenesis of the ulungur intrusive complex, NW China, and implications for crustal generation and reworking in accretionary orogens. J Petrol. https://doi.org/10.1093/petrology/egaa018

Valley JW, Kinny PD, Schulze DJ, Spicuzza MJ (1998) Zircon megacrysts from kimberlite: oxygen isotope variability among mantle melts. Contrib Miner Petrol 133:1–11

Valley JW, Lackey JS, Cavosie AJ, Clechenko CC, Spicuzza MJ, Basei MAS, Bindeman IN, Ferreira VP, Sial AN, King EM, Peck WH, Sinha AK, Wei CS (2005) 4.4 Billion years of crustal maturation: oxygen isotope ratios of magmatic zircon. Contrib Miner Petrol 150:561–580

Vervoort JD, Patchett PJ, Soderlund U, Baker M (2004) Isotopic composition of Yb and the determination of Lu concentrations and Lu/Hf ratios by isotope dilution MC-ICP-MS. Geochem Geophys Geosyst 5:Q11002

Wiedenbeck M, Alle P, Corfu F, Griffin WL, Meier M, Von Quadt A, Roddick JC, Spiegel W (1995) Three natural zircon standards for U-Th-Pb, Lu-Hf, trace element and REE analyses. Geostand Newsl 19:1–23

Wilhem C, Windley BF, Stampfli GM (2012) The Altaids of Central Asia: a tectonic and evolutionary innovative review. Earth Sci Rev 113:303–341

Windley BF, Alexeiev D, Xiao WJ, Kröner A, Badarch G (2007) Tectonic models for accretion of the Central Asian Orogenic Belt. J Geol Soc Lond 164:31–47

Xia XP, Sun M, Geng HY, Sun YL, Wang YJ, Zhao GC (2011) Quasi-simultaneous determination of U-Pb and Hf isotope compositions of zircon by excimer laser-ablation multiple-collector ICPMS. J Anal Spectrom 26:1868–1871

Xiao WJ, Windley BF, Badarch G, Sun S, Li JL, Qin KZ, Wang ZH (2004) Palaeozoic accretionary and convergent tectonics of the southern Altaids: implications for the growth of Central Asia. J Geol Soc 161:339–342

Xiao WJ, Windley BF, Yuan C, Sun M, Han CM, Lin SF, Chen HL, Yan QR, Liu DY, Qin KZ, Li JL, Sun S (2009) Paleozoic multiple subduction–accretion processes of the southern Altaids. Am J Sci 309:221–270

Xie LW, Zhang YB, Zhang HH, Sun JF, Wu FY (2008) In situ simultaneous determination of trace elements, U-Pb and Lu-Hf isotopes in zircon and baddeleyite. Chin Sci Bull 53:1565–1573

Ye XT, Zhang CL, Zou HB, Yao CY, Dong YG (2017) Age and geochemistry of the Zhaheba ophiolite complex in eastern Junggar of the Central Asian Orogenic Belt (CAOB): implications for the accretion process of the Junggar terrane. Geol Mag 154:419–440

Zhang ZC, Zhou G, Kusky TM, Yan SH, Chen BL, Zhao L (2009) Late Paleozoic volcanic record of the Eastern Junggar terrane, Xinjiang, Northwestern China: major and trace element characteristics, Sr–Nd isotopic systematics and implications for tectonic evolution. Gondwana Res 16:201–215

Zhang YY, Sun M, Yuan C, Long XP, Jiang YD, Li PF, Huang ZY, Du L (2018) Alternating trench advance and retreat: Insights from Paleozoic magmatism in the eastern Tianshan, Central Asian Orogenic Belt. Tectonics 37:2142–2164